physica status solidi a
www.pss-a.com

Check for updates

Anisotropy and Mechanistic Elucidation of Wet-Chemical Gallium Nitride Etching at the Atomic Level

*Markus Tautz, Andreas Weimar, Christian Graßl, Martin Welzel, and David Díaz Díaz**

Etching of gallium nitride is a key step in the production of blue and white light-emitting diodes (LEDs). Etching in aqueous KOH solution creates a rough surface on the LED chip to facilitate outcoupling of the photons generated, drastically increasing the resulting LED's efficiency. Compared with the common technique of dry etching, wet-chemical etching using aqueous KOH solution has significant advantages, e.g., lower complexity and cost and less remaining surface damage. An in-depth analysis of the molecular etch reaction by characterization of the reaction products is reported. The mechanism identified explains the cause of anisotropic etching, which leads to the formation of hexagonal pyramids. The concept of hydroxide repulsion by protruding NH and NH_2 groups established in the literature is adapted and further developed. The susceptibility of several polar, semipolar, and nonpolar crystal facets may also be explained, as well as the commonly observed increase in average pyramid size over etch time.

1. Introduction

Gallium nitride has been successfully used for the production of blue and white light-emitting diodes (LEDs) for the last 30 years.[1] With a direct bandgap of $E_g = 3.5$ eV, GaN emits UV light with a wavelength of 365 nm upon application of voltage.[2] Insertion of an $In_xGa_{1-x}N$ multiquantum well (MQW) can increase LED efficiency and shift the emission wavelength into the range of blue visible light.[3] During standard GaN LED production, GaN is grown via metalorganic chemical vapor deposition (MOCVD).[4] Epitaxy describes deposition of a material—in this study, GaN—on a substrate. The material deposited can be identical (homoepitaxy) or different (heteroepitaxy) from the grown material. For cost efficiency, GaN LEDs are typically produced in a heteroepitaxial approach on sapphire (Al_2O_3) substrates.[5] During epitaxial growth, the crystal lattice of the substrate is transferred to GaN.

Sapphire has a relatively low thermal conductivity; thus, the performance of the final LED chip is limited because the heat generated by the operating device cannot be dissipated. A common approach to produce high-power LEDs is "flip-chip" technology,[6] in which a silicon substrate wafer is bonded on the top surface of the epitaxial GaN layer. The initial electrical and adhesive connection is made by a soldered metal layer stack. In the next step, laser lift off (LLO) is applied to the back of the sapphire substrate.[7,8] The irradiation wavelength of the laser is chosen to fall between the bandgap energies of the sapphire and GaN to allow light to cross the sapphire substrate and be absorbed by the GaN layer. The induced energy causes the GaN nearest the sapphire substrate to thermally decompose to Ga and gaseous nitrogen. The volume increase caused by the liberation of nitrogen causes separation of the sapphire substrate and GaN.

To further enhance the flip-chip LED performance, the revealed GaN surface is addressed during processing. The refractive indices of GaN and air have values of ≈2.5 and 1.0, respectively;[9] this discrepancy results in a light escape cone of 23.6°. Generated photons directed outside of this angle, toward the chip surface, suffer total reflection. They are absorbed in the sidewall of the LED and do not participate in light emission, which effectively decreases the LED's efficiency. Surface roughening has been a common approach to increase the outcoupling probability for photons for decades, which we recently reviewed.[10] A rough surface supplies a larger total surface area, as well as additional surface angles with varying orientations through which photons can cross.

Immersion in aqueous KOH solution at elevated temperature is a common technique for wet-chemical GaN roughening.[11] In an anisotropic etch process, the hexagonal crystal lattice leads to formation of hexagonal pyramids on an N-polar GaN surface.[12] On a Ga-polar surface, etching occurs exclusively at dislocation

Dr. M. Tautz, Dr. A. Weimar, Dr. C. Graßl, Dr. M. Welzel
OSRAM Opto Semiconductors GmbH
Leibnizstr. 4, 93053 Regensburg, Germany

Dr. M. Tautz, Prof. D. Díaz Díaz
Institut für Organische Chemie
Universität Regensburg
Universitätsstr. 31, 93053 Regensburg, Germany

Prof. D. Díaz Díaz
Departamento de Química Orgánica
Universidad de La Laguna
Avda. Astrofísico Francisco Sánchez 3, 38206 La Laguna, Tenerife, Spain
E-mail: ddiazdiaz@ull.edu.es

Prof. D. Díaz Díaz
Instituto de Bio-Orgánica Antonio González
Universidad de La Laguna
Avda. Astrofísico Francisco Sánchez 2, 38206 La Laguna, Tenerife, Spain

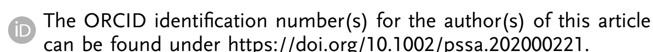
The ORCID identification number(s) for the author(s) of this article can be found under https://doi.org/10.1002/pssa.202000221.

© 2020 The Authors. Published by Wiley-VCH GmbH. This is an open access article under the terms of the Creative Commons Attribution License, which permits use, distribution and reproduction in any medium, provided the original work is properly cited.

Correction added on 11 September 2020, after first online publication: Projekt Deal funding statement has been added.

DOI: 10.1002/pssa.202000221

sites. The disrupted crystal bonds in these positions cause etch removal. Etch process conditions influence the etch mechanism, including the impact of dislocations. Dislocations had no impact during N-polar GaN etching without above-bandgap illumination and without application of bias voltage.[13] Under the same conditions, Ga-polar material generates etch pits at dislocation sites. This phenomenon has frequently been exploited for atomic force microscopy (AFM) analysis of dislocation density.[14]

A formal substitution reaction path has been reported as the mechanism of wet-chemical GaN etching,[13,15,16] meaning the formal oxidation states of Ga and N remain unchanged during etching. In terms of the reaction product, both Ga_2O_3 and $Ga(OH)_3$ have been suggested

$$2GaN + 3H_2O \rightarrow Ga_2O_3 + 2NH_3 \quad (1)$$

$$GaN + 3H_2O \rightarrow Ga(OH)_3 + NH_3 \quad (2)$$

Under different process conditions, a different mechanism is conceivable: the field of photoelectrochemical (PEC) etching entails application of above-bandgap illumination and bias voltage.[17] Light illumination generates electron–hole pairs. The use of positive polarization also increases the availability of holes generated by illumination to support the oxidation partial reaction. Several papers have reported a redox approach as the mechanism for PEC etching, in agreement with the concept of anodic dissolution of other semiconducting materials.[18,19]

$$2GaN + 6h^+ \rightarrow 2Ga^{3+} + N_2 \quad (3)$$

$$6H^+ + 6e^- \rightarrow 3H_2 \quad (4)$$

In this mechanism, Ga remains at a formal oxidation state of +3, whereas N^{3-} is reduced to gaseous N_2. Which etch mechanism occurs during etching without application of bias voltage and above-bandgap illumination has remained an open question to this point.

Anisotropic etching has also been discussed in the literature. The angles of the hexagonal pyramids that evolve during N-face GaN etching have been reported to have a ≈60° angle toward the $(000\bar{1})$ lateral N-face.[12,20,21] Palacios and co-workers[21] suggested that the pyramid side planes consist of $\{11\bar{2}1\}$ crystal facets. Several later reports concluded that $\{10\bar{1}\,\bar{1}\}$ facets form the pyramid side planes. The difference in the etch behavior between N-face and Ga-face GaN has been explained with a model of repulsion between protruding nitrogen and incoming OH^- ions.[14,16,22] Both surface-standing nitrogen and OH^- are negatively charged, which was suggested to cause electronic hindrance. On a Ga-polar surface, nitrogen atoms protrude at a 90° angle from the surface, creating considerable steric hindrance.

In this report, we analyzed the molecular etch reaction of GaN under dark and current-free conditions to characterize the reaction products. Based on the results, we explain the previously reported phenomena observed during GaN etching (e.g., the decrease in etch rate at very high and low concentrations of KOH).[21] In addition, we build upon the previously reported model of hydroxide repulsion to explain the relative stability of several semipolar and nonpolar crystal facets, including the pyramid side planes formed during N-face GaN etching.

2. Results and Discussion

2.1. Substitution Mechanism under NH_3 Formation

Previous reports have debated the molecular reaction mechanism of GaN etching.[10,13,15,16] Three separate experimental approaches in this work allowed clarification of the mechanism.

2.1.1. Analysis of Reaction Products

In a first experiment, the formation of gaseous reaction products during etching was investigated. A 15.24 cm GaN wafer was pretreated in buffered oxide etch (BOE) solution to remove Ga and GaO_x residues from LLO and ensure that no side reaction might lead to gas bubble formation on the wafer's surface. The wafer was subsequently immersed in aqueous KOH solution (30 wt%) at a temperature of 80 °C. A GaN etch rate of 138 ± 17 nm min^{-1} was expected (mean ± standard deviation, $n = 5$),[23] which translates to a material removal rate of 0.174 mg min^{-1}. Assuming the hypothesized redox mechanism of N_2 and H_2 formation, the combined amount of formed gas would be 4.13×10^{-6} mol min^{-1}.

The back of the GaN wafer was protected from KOH etching by a 20 nm Pt layer. However, Si was accessible on the wafer side walls. Inductively coupled plasma-optical emission spectrometry analysis revealed a Si etch rate of 1185 ± 99 nm min^{-1}.[23] Although Si was accessible to solution only in a small area on the wafer side wall, bubble formation caused by H_2 production was clearly observed. No bubble formation was visible on the GaN surface. From this preliminary experiment, it was concluded that no N_2 or H_2 formation occurred during the etch reaction of GaN.

Subsequently, the formation of NH_3 during the etch reaction was analyzed. First, the pH change in the atmosphere above the solution was monitored. To detect the evolution of NH_3, wet pH indicator stripes were placed inside the vials above the KOH solution. Three individual entries contained aqueous KOH (20 mL, 30 wt%) with a 1 × 2 cm polished GaN sample in solution at room temperature. Three further control entries contained only KOH solution without GaN. All vials were closed and slowly heated to 50 °C to gradually accelerate the etch reaction. During heating, the pH indicator stripes showed a pH change from 7 to 12 above the KOH solutions containing GaN (**Figure 1**b). The control experiments (without GaN) showed no pH change (Figure 1a), meaning no KOH evaporated from the solution, and the formation of NH_3 caused the pH increase resulting from GaN etching.

In a second in-depth experimental approach, NH_3 formation was investigated by the Berthelot reaction. In its first step, the Berthelot reaction describes the oxidation of NH_3 to NH_2Cl by NaOCl.[24] In the second step, NH_2Cl reacts with thymol to form a blue indole dye via formation of a combined π-electron system. The conditions and results are shown in **Table 1**, and the appearance of the aqueous and organic phases for the various conditions is shown in **Figure 2**.

The control reaction with only KOH, NaOCl, and thymol (Table 1, entry 1) had a colorless aqueous phase and a brown organic phase. The latter appeared after the addition of thymol, presumably due to decomposition in 80 °C KOH solution.

© 2020 The Authors. Published by Wiley-VCH GmbH

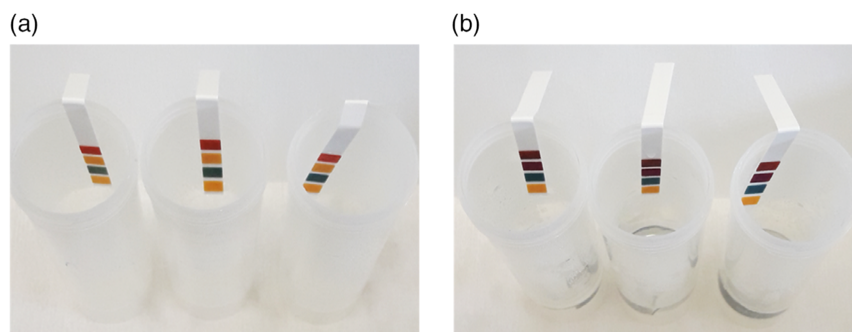

Figure 1. Images of wet pH indicator stripes placed above aqueous KOH solution (20 mL, 30 wt%) a) without and b) with polished MOCVD GaN samples. The samples were prepared at room temperature, closed, and slowly heated to 50 °C. NH_3 formed by the etching reaction evaporated from the solution and caused a pH change from 7 to 12 in the vials containing GaN. The control experiments without GaN showed no pH change, proving that KOH did not evaporate.

Table 1. Berthelot reaction experiments for NH_3 detection in aqueous KOH solution at 80 °C. All entries contained KOH (20 mL, 30 wt%), NaOCl solution (100 µL), and ≈10 mg thymol (spatula tip).

Entry	NH_3 [µL]	GaN/Si sample	Appearance aqueous phase	Appearance organic phase
1	–	–	Colorless	Brown
2	100	–	Yellow	Blue
3	–	5.08 cm GaN pieces	Yellow	Brown
4	–	5.08 cm GaN ground	Yellow	Brown
5	–	Polished MOCVD GaN	Yellow	Blue
6	–	Si substrate	Colorless	Brown

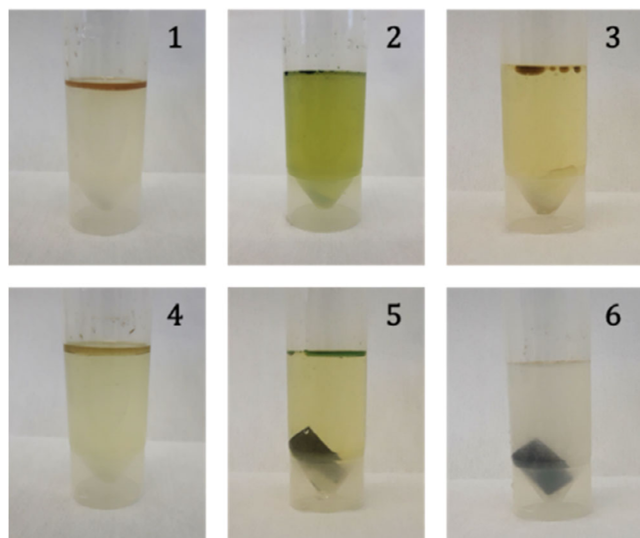

Figure 2. Images of Berthelot reaction entries 1–6 for detection of NH_3 during GaN etching. In all entries, KOH (20 mL, 30 wt%) was preheated to 80 °C. Thereafter, NaOCl solution (100 µL) and ≈10 mg thymol (spatula tip) were added. The entry numbers refer to Table 1. A blue organic phase on top of the aqueous solution was observed for the polished epitaxial GaN sample as well as the control experiment, in which exogenous NH_3 was added to the KOH solution.

In another reaction (entry 2), NH_3 (100 µL, 28 wt%) was directly added to the hot reagent mixture. This led to yellow discoloration of the aqueous phase, with a blue color observed in the organic phase, as expected in the presence of NH_3.

Pieces of a 5.08 cm molecular beam epitaxy (MBE)-grown bulk GaN substrate wafer were added to the reagent mixture for the third reaction (entry 3). No blue color was visible in the organic phase. The addition of ground MBE GaN (entry 4) also did not lead to a blue organic phase, though the aqueous phase had a slightly yellow color in both cases.

The MBE GaN samples had a low etch rate due to saturation of the N-face with $\{10\bar{1}\,\bar{1}\}$ pyramids prior to etching. Polished bulk MOCVD-grown GaN was used (entry 5) to achieve a higher etch rate. Due to the polishing process, the initial GaN N-face was terminated by the quickly etched $(000\bar{1})$ crystal facet. This experiment (entry 5) appears essentially the same as the control experiment (entry 2) to which NH_3 was added directly. NH_3 formation was thus confirmed by the Berthelot reaction, at least in the case of GaN etching at the etch rate achieved by the polished MOCVD GaN sample. It seems likely that the sensitivity of the experimental design was too low to also detect the small concentrations of NH_3 formed by slower etching reactions (i.e., that of MBE GaN).

2.1.2. Molecular Reaction Mechanism

The formation of NH_3 during the etch reaction was confirmed by the three experiments described to this point. This allowed the previously reported reaction mechanisms to be narrowed to two alternatives

$$2GaN + 3H_2O \rightarrow Ga_2O_3 + 2NH_3 \quad (5)$$

$$GaN + 3H_2O \rightarrow Ga(OH)_3 + NH_3 \quad (6)$$

At this point, the only difference between both mechanistic approaches is the gallium–oxygen species formed. Nucleophilic attack of hydroxide ions in the solution on positively charged Ga atoms is a feasible first reaction step, and has been previously reported to create Ga—OH bonds.[16] It has also been reported that $Ga(OH)_3$ dissolves readily in acidic and alkaline solutions, with formation of $[Ga(H_2O)_6]^{3+}$ and $[Ga(OH)_4]^-$, respectively.[25]

 © 2020 The Authors. Published by Wiley-VCH GmbH

Ga_2O_3 is generally formed from $Ga(OH)_3$ by dehydration.[25] The formation of Ga_2O_3 would, therefore, require further reaction after the initial formation of Ga—OH bonds, which would not be feasible due to the solubility of $Ga(OH)_3$ in water. Of the Ga species present in solution, only $[Ga(OH)_4]^-$ is present at high pH. Thus, the net reaction of GaN etching at the reaction conditions applied in this study must be

$$GaN + 3H_2O + OH^- \rightarrow Ga(OH)_4^- + NH_3 \quad (7)$$

The step-by-step removal of GaN, in cycles of Ga—O bond formation and dissolution of the reaction products, has been extensively discussed in previous studies.[16,22,26]

At this point, it must be clarified that the postulated reaction mechanism was found under these specific conditions; other mechanisms are possible under other conditions. For instance, diffusion limitation has been reported under PEC conditions.[17,27,28] It is possible that the reaction mechanism changes once holes are generated by above-bandgap illumination. Further experiments regarding the reaction mechanism should include a detailed study of the transition between NH_3 formation and N_2/H_2 formation.

2.2. Explanation for Anisotropic Etching at the Atomic Level

The root cause for the development of pyramids during KOH etching was investigated at the atomic level.

2.2.1. Characterization of Pyramid Side Facet Species

AFM measurement was applied to precisely determine the species of formed pyramid side facets as a first step toward explaining the anisotropic etch behavior of GaN. The angle between the side facets and the lateral $(000\bar{1})$ N-face was determined to be $61.5 \pm 0.6°$ by AFM (**Figure 3**).

Based on the lattice constants of wurtzite GaN, the theoretical angle between $\{10\bar{1}\,\bar{1}\}$ and $(000\bar{1})$ crystal facets is 62.1°; thus, the theoretical and actual angles were in good agreement. This result indicates that the pyramid side facets represent the $\{10\bar{1}\,\bar{1}\}$ planes.

2.2.2. Selectivity of N-Face over Ga-Face Etching

GaN reacts under dissociative water adsorption once it is immersed in aqueous KOH.[17] Protons bond to the negatively charged nitrogen, whereas the Ga-polar surface is terminated by hydroxide ions. The schematic surface states of both polarities are shown in **Figure 4**, where the Ga—N, Ga—O, O—H, and N—H bond lengths are pictured to scale with the literature values of 1.96, 1.92, 0.98, and 1.01 Å, respectively.[29–37]

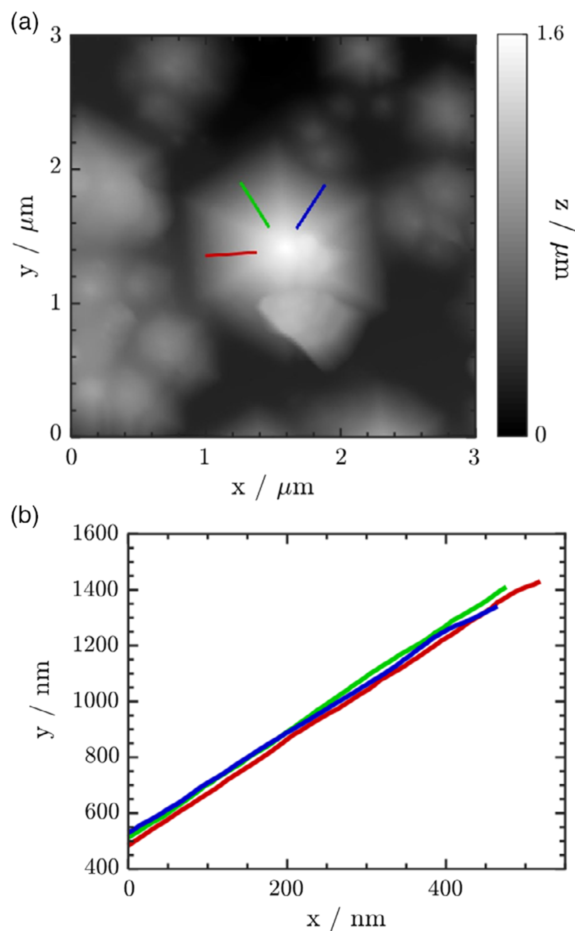

Figure 3. a) AFM image of single MOCVD GaN pyramid after 6 min in aqueous KOH solution (30 wt%) at 80 °C. b) The three lines indicate the cross sections of the pyramid side facets. Height diagram of the cross sections. The angle of the side facets relative to the base plane was determined to be $61.5 \pm 0.6°$, which aligns well with the theoretical angle of 62.1°, which $\{10\bar{1}\,\bar{1}\}$ facets form with the base plane.

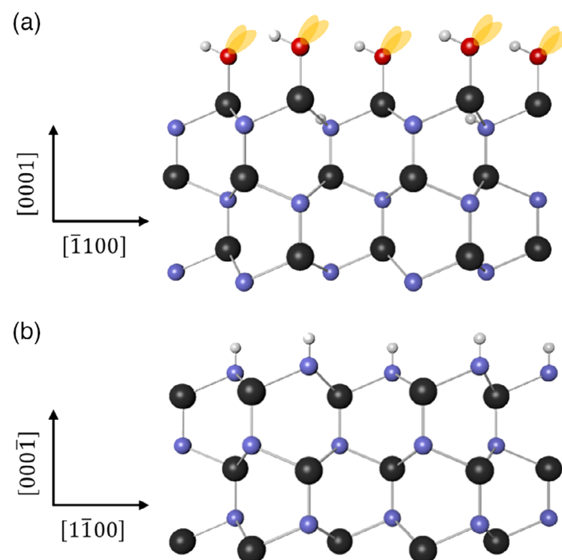

Figure 4. a) Schematic surfaces of Ga-polar (0001) and b) N-polar $(000\bar{1})$ crystal polarities on the atomic level. The top face of each schematic represents the surface. Hydroxide ions are adsorbed to the Ga-polar surface, whereas protons bond to nitrogen, a phenomenon referred to as dissociative water adsorption. Black, blue, red, and white spheres represent Ga, N, O, and H, respectively. Surface-standing free electron pairs are indicated as orangish ellipses.

© 2020 The Authors. Published by Wiley-VCH GmbH

Before etching begins, the first layer of Ga atoms is easily accessible to hydroxide ions in solution. The reaction mechanism established in this work means the first Ga atom layer is then removed, meaning hydroxide ions are blocked by the now-exposed NH_2 groups (**Figure 5**, bottom).

NH_2 groups protrude at a vertical 90° angle from the Ga-polar surface. This concept of hydroxide repulsion has been previously reported.[11] Briefly, the two hydrogen atoms present on every nitrogen provide steric blocking, and the free electron pair on each nitrogen provides electronic blocking. In contrast, the initial N-polar surface is terminated with NH groups (**Figure 6**, top). The nitrogen atoms on the surface bond to only one hydrogen, and do not have a free electron pair. This decreases the blocking of the Ga-polar crystal surface. The angle between the Ga—N bond and the lateral N-face is only 19°, compared with 90° for the Ga-face. In consequence, hydroxide ions can attack Ga, as shown in Figure 6, bottom. Once an entire GaN layer is removed, the initial surface condition present prior to etching removal is recovered. Etching of N-face GaN can thus proceed at a higher rate.

2.2.3. Stability of Pyramid Side Facets

Etch selectivity between Ga- and N-face GaN was further examined in terms of the stability of semipolar $\{10\bar{1}\,\bar{1}\}$ pyramid side facets. The formation of hexagonal pyramids is a consequence of a higher stability of the $\{10\bar{1}\,\bar{1}\}$ crystal facets compared with the N-polar $(000\bar{1})$ plane. The pyramid facets were theoretically investigated to examine the surface termination on the atomic level (**Figure 7**).

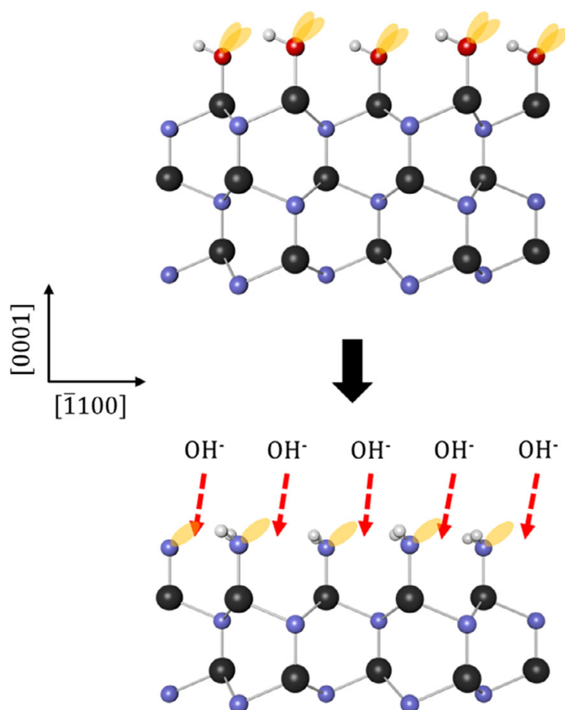

Figure 5. Removal of a single Ga atom layer from the Ga-polar (0001) GaN surface results in the termination of the remaining surface, with NH_2 groups protruding at a 90° angle relative to the lateral Ga-face. Approaching negatively charged hydroxide ions are blocked by steric and electronic repulsion from negatively polarized NH_2 groups. In addition to the two hydrogen atoms on every protruding nitrogen atom, a nonbonding electron pair is also present, providing further electronic hindrance.

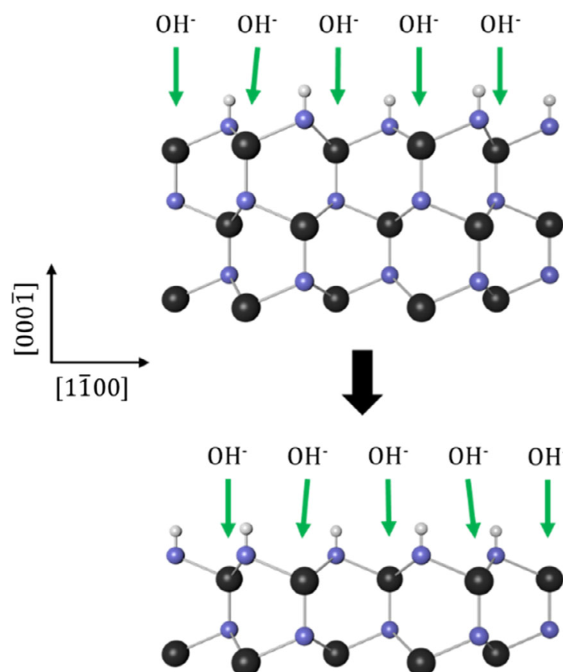

Figure 6. Removal of a single GaN atom layer from the N-polar $(000\bar{1})$ GaN surface results in the termination of the remaining surface with NH groups protruding at a 19° angle relative to the lateral N-face. Approaching negatively charged hydroxide ions are blocked less effectively than when approaching the Ga-face, which leads to material removal during etching.

The NH_2 groups protrude from the surface with alternating angles of 79° and 35.5°. Therefore, the magnitude of the blocking against approaching hydroxide ions was expected to fall between that of the Ga- and N-faces. This relative etch selectivity conforms to the empirically observed etch behavior.

During etch experiments performed with N-polar and polished MOCVD GaN, additional crystal facets were observed

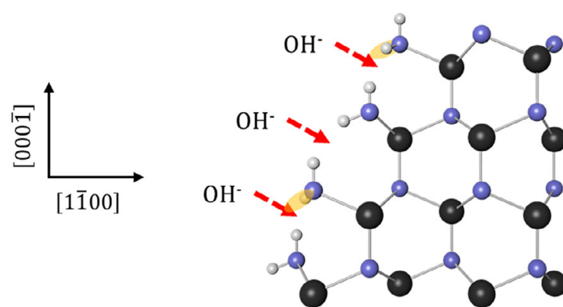

Figure 7. Schematic surface of $\{10\bar{1}\,\bar{1}\}$ pyramid side facets. NH_2 groups protrude from the surface at alternating angles of 79° and 35.5°. This situation implies relative etch selectivity between N-face and Ga-face GaN in good agreement with actual etch behavior.

© 2020 The Authors. Published by Wiley-VCH GmbH

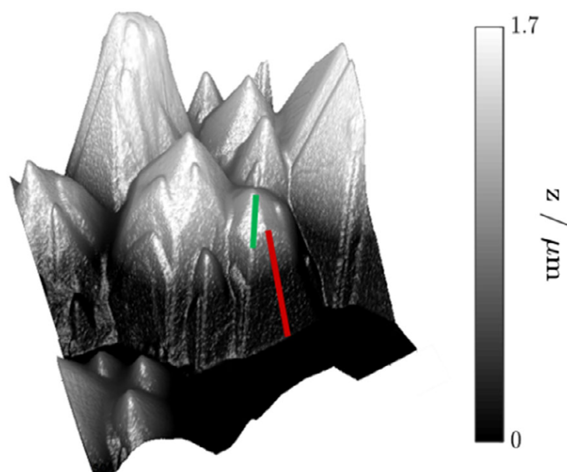

Figure 8. AFM measurement of N-polar MOCVD GaN sample after etching in aqueous KOH solution (30 wt%) at 80 °C for 6 min. The red line marks a cross section of a regular $\{10\bar{1}\bar{1}\}$ pyramid side facet. The green line indicates the presence of an additional set of crystal planes with an orientation rotated 30°.

on top of $\{10\bar{1}\bar{1}\}$ pyramids at a lower angle toward the lateral N-face in some cases (**Figure 8**, green cross section).

An angle of $38.2° \pm 0.7°$ relative to the lateral N-face was determined. Considering the 30° rotation of the additional crystal facets in the lateral direction, the $\{1\bar{2}1\bar{4}\}$ crystal facets were identified to represent the observed angle with a theoretical value of 39.2°. The latter angle was calculated from theoretical GaN crystal lattice parameters.

In the schematic view of this crystal facet, a terraced structure was obvious with alternating situations discussed in Section 2.2.2 for $(000\bar{1})$ and $\{10\bar{1}\bar{1}\}$ facets (**Figure 9**).

While etching is fast on the horizontal $(000\bar{1})$ N-face plateaus, the effective hydroxide blocking by NH_2 groups in the angled sections, reminiscent of the $\{10\bar{1}\bar{1}\}$ situation, slows the combined etch rate. Thus, the expected etch selectivity of the $\{1\bar{2}1\bar{4}\}$ crystal facets was between the observed etch rates of the $(000\bar{1})$ and $\{10\bar{1}\bar{1}\}$ facets. In fact, this theoretical consideration was borne out by actual etch experiments; it appears that the $\{1\bar{2}1\bar{4}\}$ facets develop as an intermediate step if etching of an initial $(000\bar{1})$ GaN surface evolves into $\{10\bar{1}\bar{1}\}$ pyramids.

2.2.4. Stability of Nonpolar Crystal Facets

In the next step, the etch behavior of the nonpolar $\{1\bar{1}00\}$ crystal facets was analyzed (**Figure 10**).

Alternating NH_2 and NH groups protrude at angles of 81° and 0°, respectively. The expected relatively low etch rate was confirmed by scanning electron microscopy (SEM) analysis of a ground MBE GaN sample (**Figure 11**).

SEM images of the ground GaN powder were taken before (Figure 11a,b) and after (Figure 11c,d) etching in aqueous KOH (30 wt%) for 120 min at 80 °C. The long etch time was chosen to reach termination of the GaN particles with the most stable crystal facets. Small particles of powder present prior to etching were entirely dissolved during the etching process. Large particles within the powder showed smooth and defined crystal facets after etching, and the crystal facets were arranged in terraces. The most stable GaN facets could be identified at higher magnification (**Figure 12**).

On the bottom of the GaN particle shown, the N-polar direction was identified using the large $\{10\bar{1}\bar{1}\}$ pyramids. These pyramids transitioned into nonpolar $\{1\bar{1}00\}$ facets and terminated at Ga-polar (0001) crystal facets at a 90° angle. No other crystal planes were found at this point of the etch progress, proving that these three facets are indeed the most stable to KOH etching. The three could be ranked in terms of relative etch selectivity: the Ga-polar (0001) facet has been frequently reported to show no detectable etch progress under the process conditions applied.[10] The etch rate of $\{1\bar{1}00\}$ facets must be higher compared with $\{10\bar{1}\bar{1}\}$ pyramid side planes. If the latter selectivity were reversed, GaN pillars would form as a consequence of N-face GaN etching instead of pyramids. In this case, some surface sections would have to show areas in which the $\{10\bar{1}\bar{1}\}$ facets transition into vertical $\{1\bar{1}00\}$ facets due to a hypothetical higher resistance to etching. As this has not been observed during GaN etching under non-PEC conditions, the $\{10\bar{1}\bar{1}\}$ pyramids must have higher resistance to etching. The relative

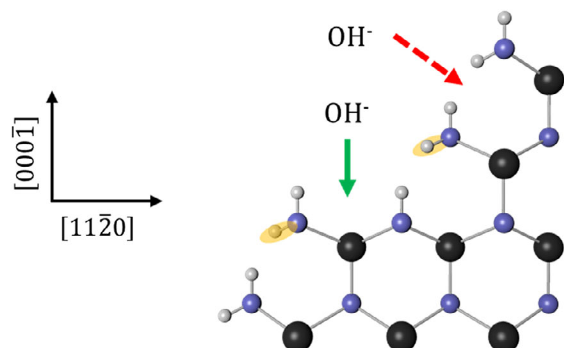

Figure 9. Schematic surface of $\{1\bar{2}1\bar{4}\}$ pyramid side facets. The situation is reminiscent of a terraced combination of alternating $\{10\bar{1}\bar{1}\}$ and $(000\bar{1})$ surface states, leading to expectation of an etch selectivity between that of $(000\bar{1})$ and $\{10\bar{1}\bar{1}\}$ facets.

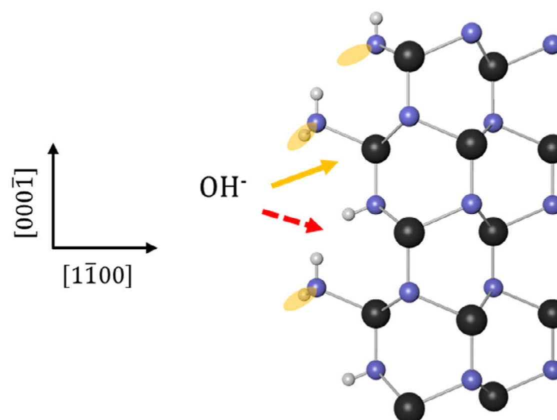

Figure 10. Schematic surface of $\{1\bar{1}00\}$ GaN surface. NH_2 groups protrude with an angle of 81° relative to the $\{1\bar{1}00\}$ surface, whereas NH groups provide additional blocking with a 0° angle relative to the surface.

© 2020 The Authors. Published by Wiley-VCH GmbH

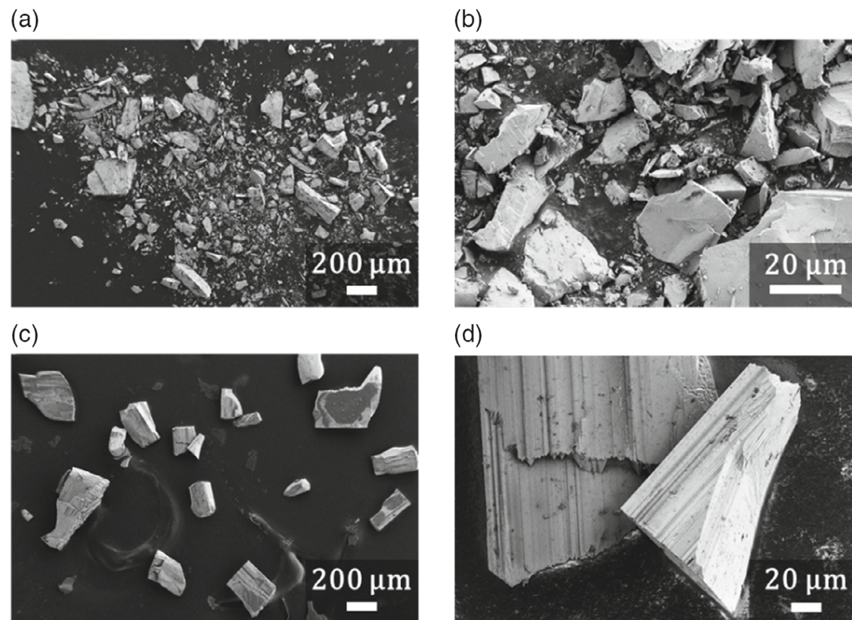

Figure 11. SEM images of ground MBE-grown bulk GaN particles a,b) before and c,d) after etching in aqueous KOH solution (30 wt%) at 80 °C for 120 min. Small particles were entirely dissolved during etching. The remaining larger particles have smooth crystal facets arranged in terraces.

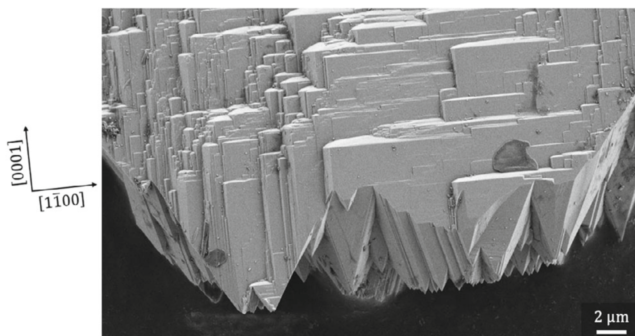

Figure 12. High magnification SEM image of a grinded MBE-grown bulk GaN particle after etching in aqueous KOH solution (30 wt%) at 80 °C for 120 min. The N-polar crystal direction is visible on the bottom of the sample by means of large $\{10\bar{1}\,\bar{1}\}$ pyramids. These terminated in nonpolar $\{1\bar{1}00\}$ crystal facets. In Ga-polar direction, $\{1\bar{1}00\}$ facets ended at terraced (0001) plateaus. No other facets had remained at this stage of etch duration.

susceptibility of the three most stable crystal facets can thus be determined to be $\{1\bar{1}00\} > \{10\bar{1}\,\bar{1}\} > (0001)$. Compared with these, the N-polar $(000\bar{1})$ facet disappears after a relatively short period of etching. The empirically observed stability agrees with the theoretical considerations discussed by means of schematic GaN surface models on the atomic level.

2.2.5. Instability of Pyramid Tips during Prolonged Etching

Etching of N-polar GaN in aqueous KOH solution has previously been reported to occur in a steady equilibrium of pyramid formation, coalescence, and erosion of the pyramid tips.[20] The breakdown of pyramid tips again leads to the formation of smaller pyramids. Thus, the most stable particle morphology during etching is expected to have large and smooth crystal facets, and a lower relative etch resistance is expected at transitions from one facet to another. Thus, the pyramid size should become as large as possible to provide the highest possible stability.

However, during etch experiments, pyramids were found to be eroded after etching for no more than 2 min. SEM analysis of an N-polar MOCVD GaN sample surface section in 1 min steps during etching (aqueous KOH solution [30 wt%] at 80 °C) showed the growth and breakdown of a large pyramid (**Figure 13**).

The relative instability of pyramid tips was further analyzed schematically (**Figure 14**).

While the pyramid side walls are formed by the stable $\{10\bar{1}\,\bar{1}\}$ crystal facets, the tip is equivalent to a microscopic $(000\bar{1})$ N-face plateau. Thus, the tendency of the material to form large homogeneous crystal facets is disrupted. During etching, the combination of formation and breakdown of large crystal facets leads to a steady but slow increase in average pyramid size, a finding in agreement with several previous reports.[12,20,21]

3. Conclusions

In this study, we investigated the GaN etch process in aqueous KOH solution in detail. First, the molecular reaction mechanism was elucidated using three independent experimental approaches to prove that NH_3 evolves during etching. This allowed the mechanism in aqueous solution under the specific reaction conditions applied to be narrowed down to one possibility. By changes in the electrostatics of the crystal by application of bias voltage and above-bandgap illumination

© 2020 The Authors. Published by Wiley-VCH GmbH

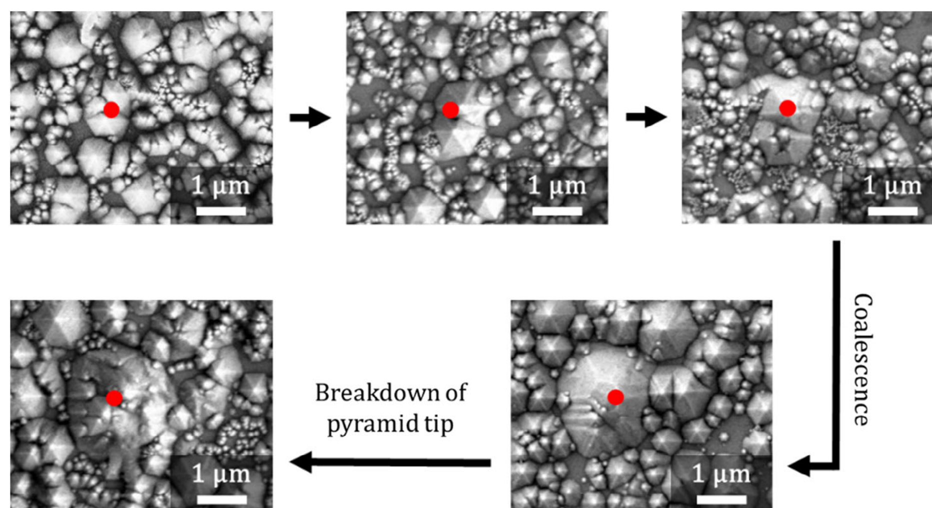

Figure 13. Consecutive SEM images of the same surface of a MOCVD-grown N-face GaN etched in 1 min steps in aqueous KOH solution (30 wt%) at 80 °C. The observed pyramid had grown to its maximum size in the fourth image. After 1 min prolonged etch time, the tip of the pyramid had broken down, leading to the development of smaller pyramids.

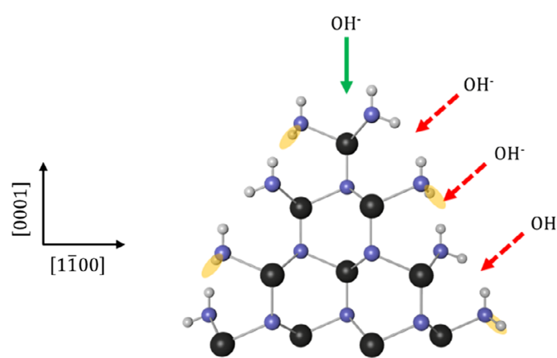

Figure 14. Schematic tip of $\{10\bar{1}\,\bar{1}\}$ GaN pyramid on the atomic level. Directly on the tip, a microscopic $(000\bar{1})$ is visible. This explains the relative instability of the pyramid tip, which leads to the breakdown of large pyramids.

(e.g., by PEC etching), the mechanism might change to a combination of N^{3-} oxidation and H^+ reduction—equivalent to the concept of anodic dissolution of other common semiconductors.

The underlying reasons for the observed anisotropic etch behavior of GaN were analyzed at the atomic level. Based on theoretical and schematic considerations, the concept of hydroxide repulsion by protruding nitrogen established in the literature was further examined. The etch selectivity of the most stable GaN crystal facets could be explained. Etching of grinded MBE-grown bulk GaN led to the conclusion that the most stable crystal facets against KOH etching are $\{1\bar{1}00\} < \{10\bar{1}\,\bar{1}\} < (0001)$. The observed breakdown of pyramid tips can be explained by the presence of a microscopic N-face $(000\bar{1})$ plateau with a relatively high etch rate on each pyramid tip. While the stability of the GaN surface is increased by the presence of large facets, the maximum pyramid lifetime was found to be 2 min under the reaction conditions used. Etching of GaN thus occurs as a steady equilibrium of pyramid formation and breakdown, which causes a slow and steady increase of the average pyramid size during etching. Thus, the exact positions of the pyramid tips on the surface undergo constant change.

4. Experimental Section

Materials: Selectipur grade KOH was purchased from BASF. Planar sapphire wafers were used as growth substrates during epitaxy. Silicon wafers were purchased from Siltronic. Commercially available MBE-grown 5.08 cm bulk GaN wafers with a threading dislocation density of 2.0×10^6 cm^{-2} were used. Indicator strips for pH were purchased from Roth. GPR Rectapur grade NaOCl (14 wt% active Cl_2 in aqueous solution) and analytical grade thymol were used as received from VWR. BOE solution with HF (4.15 wt%) and NH_4F (33 wt%) and no surfactants or additives was obtained from Honeywell.

Preparation of Epitaxial GaN Samples: Standard c-plane oriented GaN epilayers were grown using commercially available Veeco MOCVD tools. After deposition of a thin AlN nucleation layer, a 3 µm bulk GaN layer was deposited in the Ga-polar direction. The dislocation density was determined by photoluminescence microscopy (PLM) to be approximately 4×10^8 cm^{-2}. Due to the high dislocation density, this value represents a minimum, as PLM images showed dislocation aggregation.[23] For PLM analysis, a rudimentary GaN/$In_xGa_{1-x}N$ MQW was deposited on the GaN, though these wafers were not used for the etch experiments discussed later.

After epitaxial growth, the Ga-face of the epilayer was bonded to a silicon substrate with a nonohmic metal contact to achieve electrical isolation and thus avoid substrate influence on the etch process. The sapphire was removed by LLO to reveal the N-polar $(000\bar{1})$ crystal facet. The silicon back of the wafers was protected against KOH etching by deposition of a 20 nm Pt layer.

A set of samples underwent surface polishing; LLO surface roughness was removed using a commercially available wafer polisher. An aqueous alkaline slurry (pH 12.3) was used in combination with a mechanical component based on SiO_2 particles. This process decreased surface roughness (R_q) from 24.1 to 1.1 nm, as measured by AFM.

Etching: Etching was conducted with full 15.24 cm MOCVD GaN wafers, with cut samples with dimensions of 1 × 2 cm, and with commercially available MBE-grown bulk GaN samples. Etching of 15.24 cm GaN wafers was conducted in a beaker. The wafers were placed on Teflon place

© 2020 The Authors. Published by Wiley-VCH GmbH

holders to allow for magnetic stirring underneath the wafer. Etching of cut 1×2 cm MOCVD GaN sample pieces, as well as ground or fragmented MBE bulk GaN, was conducted in 50 mL polypropylene centrifuge vials under magnetic stirring. The KOH solution was heated to the process temperature prior to immersion of the wafer to enable maintenance of a stable process temperature over the entire etch period.

Analytical Methods: PLM images were recorded directly after epitaxy using an Olympus BX51 microscope with an Olympus U-RFL-T UV light source. Light with a wavelength of 408 nm was used for excitation. AFM measurements were taken using a Veeco/Bruker microscope and a Scanasyst-Air tip with a 2 nm diameter. All measurements were recorded in peak force tapping mode at 2 kHz. SEM images were recorded on a Zeiss Gemini Leo 1530 microscope with an acceleration voltage of 2 keV and SE2 detection.

Acknowledgements

This work was funded by OSRAM Opto Semiconductors GmbH. The authors thank all colleagues at OSRAM Opto Semiconductors GmbH for contributing to the success of the experiments reported here. D.D.D. thanks Deutsche Forschungsgemeinschaft (DFG) for the Heisenberg Professorship Award and the Spanish Ministry of Science, Innovation and Universities for the Senior Beatriz Galindo Award (Distinguished Researcher; BEAGAL18/00166). D.D.D. thanks NANOtec, INTech, Cabildo de Tenerife, and ULL for laboratory facilities. Open access funding enabled and organized by Projekt DEAL.

Conflict of Interest

The authors declare no conflict of interest.

Keywords

anisotropy, etching, gallium nitride, light-emitting diodes, mechanism

Received: April 15, 2020
Revised: August 4, 2020
Published online:

[1] S. Nakamura, *Angew. Chem. Int. Ed.* **2015**, *54*, 7770.
[2] H. C. Yang, T. Y. Lin, Y. F. Chen, *Phys. Rev. B* **2000**, *62*, 12593.
[3] S. Nakamura, M. Senoh, N. Iwasa, S. Nagahama, *Jpn. J. Appl. Phys.* **1995**, *34*, L797.
[4] S. Nakamura, Y. Harada, M. Seno, *Appl. Phys. Lett.* **1991**, *58*, 2021.
[5] L. Liu, J. H. Edgar, *Mater. Sci. Eng. R* **2002**, *37*, 61.
[6] J. J. Wierer, D. A. Steigerwald, M. R. Krames, J. J. O'Shea, M. J. Ludowise, G. Christenson, Y.-C. Shen, C. Lowery, P. S. Martin, S. Subramanya, W. Götz, N. F. Gardner, R. S. Kern, S. A. Stockman, *Appl. Phys. Lett.* **2001**, *78*, 3379.
[7] A. David, T. Fujii, B. Moran, S. Nakamura, S. P. DenBaars, C. Weisbuch, H. Benisty, *Appl. Phys. Lett.* **2006**, *88*, 133514.
[8] W. S. Wong, T. Sands, N. W. Cheung, M. Kneissl, D. P. Bour, P. Mei, L. T. Romano, N. M. Johnson, *Appl. Phys. Lett.* **1999**, *75*, 1360.
[9] Y. Jung, J. Ahn, K. H. Baik, D. Kim, S. J. Pearton, F. Ren, J. Kim, *J. Electrochem. Soc.* **2012**, *159*, H117.
[10] M. Tautz, D. Díaz Díaz, *ChemistrySelect* **2018**, *3*, 1480.
[11] D. Zhuang, J. H. Edgar, *Mater. Sci. Eng. R* **2005**, R *48*, 1.
[12] H. M. Ng, N. G. Weimann, A. Chowdhury, *J. Appl. Phys.* **2003**, *94*, 650.
[13] W. Guo, R. Kirste, I. Bryan, Z. Bryan, L. Hussey, P. Reddy, J. Tweedie, R. Collazo, Z. Sitar, *Appl. Phys. Lett.* **2015**, *106*, 082110.
[14] T. Kozawa, T. Kachi, T. Ohwaki, Y. Taga, N. Koide, M. Koike, *J. Electrochem. Soc.* **1996**, *143*, L17.
[15] S. J. Pearton, J. J. Chen, W. T. Lim, F. Ren, D. P. Norton, *ESC Trans.* **2007**, *6*, 501.
[16] D. Li, M. Sumiya, S. Fuke, D. Yang, D. Que, Y. Suzuki, Y. Fukuda, *J. Appl. Phys.* **2001**, *90*, 4219.
[17] J. M. Hwang, J. T. Hsieh, C. Y. Ko, H. L. Hwang, W. H. Hung, *Appl. Phys. Lett.* **2000**, *76*, 3917.
[18] D. R. Turner, *J. Electrochem. Soc.* **1960**, *107*, 810.
[19] C. Youtsey, I. Adesida, G. Bulman, *Appl. Phys. Lett.* **1997**, *71*, 2151.
[20] S.-C. Han, J.-K. Kim, J. Y. Kim, K.-K. Kim, H. Tampo, S. Niki, J.-M. Lee, *J. Electrochem. Soc.* **2010**, *157*, D60.
[21] T. Palacios, F. Calle, M. Varela, C. Ballesteros, E. Monroy, F. B. Naranjo, M. A. Sánchez-García, E. Calleja, E. Muñoz, *Semicond. Sci. Technol.* **2000**, *15*, 996.
[22] M. Itoh, T. Kinoshita, C. Koike, M. Takeuchi, K. Kawasaki, Y. Aoyagi, *Jpn. J. Appl. Phys.* **2006**, *45*, 3988.
[23] M. Tautz, M. T. Kuchenbrod, J. Hertkorn, R. Weinberger, M. Welzel, A. Pfitzner, D. Díaz Díaz, *Beilstein J. Nanotechnol.* **2020**, 41.
[24] C. J. Patton, S. R. Crouch, *Anal. Chem* **1977**, *49*, 464.
[25] A. F. Holleman, E. Wiberg, N. Wiberg, *Lehrbuch Der Anorganischen Chemie*, De Gruyter, Berlin, Germany **2007**.
[26] S.-R. Xu, Y. Hao, J.-C. Zhang, X.-W. Zhou, Y.-R. Cao, X.-X. Ou, W. Mao, D.-C. Du, H. Wang, *Chin. Phys. B* **2010**, *19*, 107204.
[27] J. I. Pankove, *J. Electrochem. Soc.* **1972**, *119*, 1118.
[28] E. Harush, S. Brandon, J. Salzman, Y. Paz, *Semicond. Sci. Technol.* **2002**, *17*, 510.
[29] H. Morkoç, *Handbook of Nitride Semiconductors and Devices*, Wiley-VCH, Weinheim, Germany, **2008**.
[30] Y. Zhau, J. Davis Jr., C. S. Day, A. Lachgar, *Structural Complexity and Dimensional Flexibility of Gallium Dialkylphosphonates*, John Wiley & Sons, Inc., New York **2012**.
[31] M. Marezio, J. P. Remeika, *J. Chem. Phys.* **1967**, *46*, 1862.
[32] S. Singh, V. Jancik, H. W. Roesky, R. Herbst-Irmer, *Inorg. Chem.* **2006**, *45*, 949.
[33] W. C. Hamilton, *Acta Cryst.* **1962**, *15*, 353.
[34] S. F. Rastegar, A. A. Peyghan, H. R. Ghenaatian, N. L. Hadipour, *Appl. Surf. Sci.* **2013**, *274*, 217.
[35] L. Zhang, Y. Shao, Y. Wu, X. Hao, X. Chen, S. Qu, X. Xu, *J. Alloys Compd.* **2010**, *504*, 186.
[36] P. Visconti, K. M. Jones, M. A. Reshchikov, R. Cingolani, H. Morkoc, R. J. Molnar, *Appl. Phys. Lett.* **2000**, *77*, 3532.
[37] A. Botti, F. Bruni, S. Imberti, M. A. Ricci, A. K. Soper, *J. Mol. Liq.* **2005**, *117*, 81.

© 2020 The Authors. Published by Wiley-VCH GmbH